Approaches for land cover monitoring over Europe based on backscatter and coherence properties of Envisat and ERS SAR data

Kyriakos Ntouanoglou[1,*], Antonios Mouratidis[2]

[1] Hellenic Air Force, Greece
[2] Aristotle University of Thessaloniki, Department of Physical and Environmental Geography, Thessaloníki, Greece
* Corresponding author: kyrntouan@yahoo.gr

ABSTRACT
The purpose of this study is the exploitation of Synthetic Aperture Radar (SAR) satellite data for land cover monitoring. The properties of the recorded radar data heavily depend on the type of land cover, season and weather conditions. Therefore, it is possible to utilize the variability of these factors, in order to develop various techniques and methodologies that can be used for classifying land surfaces. In this context, this paper proposes approaches, which include the application of mathematical expressions and application of thresholds on multi-temporal data, for recognizing and classifying various types of land cover, on the basis of ERS and Envisat C-band SAR backscatter and coherence properties. These can be useful for any kind of contemporary SAR data, such as those of the current two Sentinel-1 satellites. Although this study focuses on four main land cover types (urban, mountainous, agricultural-low vegetation and forested areas) over specific areas in Europe, the same principles can be extended worldwide, leading to useful insights for designing future SAR satellite missions or for establishing guidelines for in-depth studies of specific land cover types.

KEYWORDS
remote sensing; SAR; land cover; classification; backscatter; coherence

Received: 11 January 2018
Accepted: 12 October 2018
Published online: 17 December 2018

Ntouanoglou, K., Mouratidis, A. (2018): Approaches for land cover monitoring over Europe based on backscatter and coherence properties of Envisat and ERS SAR data.
AUC Geographica 53(2), 207–219
https://doi.org/10.14712/23361980.2018.20

1. Introduction

1.1 Background and Scope

A plethora of Space-based Remote Sensing (RS) data for almost the entire Earth are nowadays available, providing access to different information for a variety of users worldwide. Land Cover (LC) classification is amongst the most popular applications of such data. Nevertheless, the "Achilles heel" of all RS-derived information is its accuracy, reliability and the challenge for their constant increase (Kaoru and Toshiharu 1996).

Land cover classification can be defined as "the ordering or arrangement of objects into groups or sets on the basis of their relationships" (Sokal 1974). Typically, the faster it is performed, the lower classification accuracy is to be expected (Ackermann 2011).

The most important factor to be considered when choosing a classification approach or designing a classification system, is the user needs. Variables such as scale, resolution and study area also have to be taken into account. In general, classification techniques can be grouped as supervised or unsupervised, hard or soft (fuzzy), per-field, sub-pixel or per-pixel and parametric or non-parametric (Lu and Weng 2007).

Additionally, it is highly advisable that the data, format and classification procedures are determined in advance. For example, if a single-date image is to be used, unlike in a time-series approach, there is no need for atmospheric corrections (Song et al. 2001). On the other hand, if the study area is rugged or mountainous, topographic correction is an important aspect to consider (Hale and Rock 2003).

An alternative to the most typically used optical (visible and infrared) bands for LC classification is the microwave (radar) part of the electromagnetic spectrum, which provides a different kind of information on the observed objects (Lusch 1999). The two main types of microwave RS are a) active and b) passive. In the former case, the radar antenna transmits its own signal and eventually records part of its return, after "reflection" on the ground surface. On the other hand, passive radar systems do not send their own signal, but only receive and record the microwave radiation emitted from the ground objects (Long 2008).

This paper deals with the active type of radar and in particular with Synthetic Aperture Radar (SAR), typically used since almost 30 years for the purposes of Earth observation from Space. Just as in optical remote sensing, there are several ways of processing and classifying SAR images. Nevertheless, a special characteristic of SAR is that – unlike optical imaging, where the user has several spectral bands available for interpretation – typically only one, two or in the best case a maximum of four bands (for fully polarimetric SAR data, which are generally rare) are available (Haack et al. 2000).

With a focus on LC classification, the objective of this study is to analyze and understand the temporal de-correlation effect of the recorded SAR signal – commonly known as backscattering, as well as the stability of the SAR signal phase – quantified as coherence values. Phase coherence is one of the main products of SAR interferometry (InSAR) and there are several factors that may affect it (Hanssen 2001):

1. The unknown integer number of phases ($2k\pi$).
2. The phase component due to topography.
3. The phase component due to distortion in the observation direction of the radar.
4. The phase component due to surface reference and errors of satellite orbit.
5. The phase component due to atmospheric delay to which the signal is subject.
6. The phase component due to any changes in the scattering characteristics of the Earth's surface between two observations.
7. The phase component due to all kinds of noise, such as thermal, the error of images writing or interference errors.

With reference to the sixth aforementioned factors, temporal changes over a ground target may occur, owing to geometric (e.g. due to wind) and/or dielectric variations (e.g. due to precipitation). This has an impact – to a different extent – on many LC types observed by a SAR sensor, which include e.g. the decrease of coherence magnitude or the increase of phase noise (Lavalle 2013). The stability of a SAR target, as denoted by the absence of backscatter and/or coherence change, may also be particularly informative and helpful for classification purposes (e.g. in the case of the built environment).

In this context, this paper proposes approaches for recognizing and classifying various types of LC, on the basis of SAR backscatter and coherence properties.

The study areas, in each of which the focus is on a particular type of terrain (urban, mountainous, agricultural and low vegetation areas, forests), are spread across Europe (Fig. 1).

In all cases, Envisat/ASAR Single Look Complex (SLC) data have been used, with the exception of forested areas, where the use of ERS data has been employed. The processing of the SAR data has been carried out using the Next ESA SAR Toolbox (NEST) and the ENvironment for Visualizing Images (ENVI™) software.

In order to process SAR images and classify them, there are several steps to be followed. One drawback of radar imaging is the lack of many different spectral bands for each acquisition. Nevertheless, alternative approaches, based on the inherent properties of the SAR signal, can be employed for tackling this obstacle. Thus, before proceeding to the description of the methodological approach of this study, a short description of relevant SAR characteristics is presented.

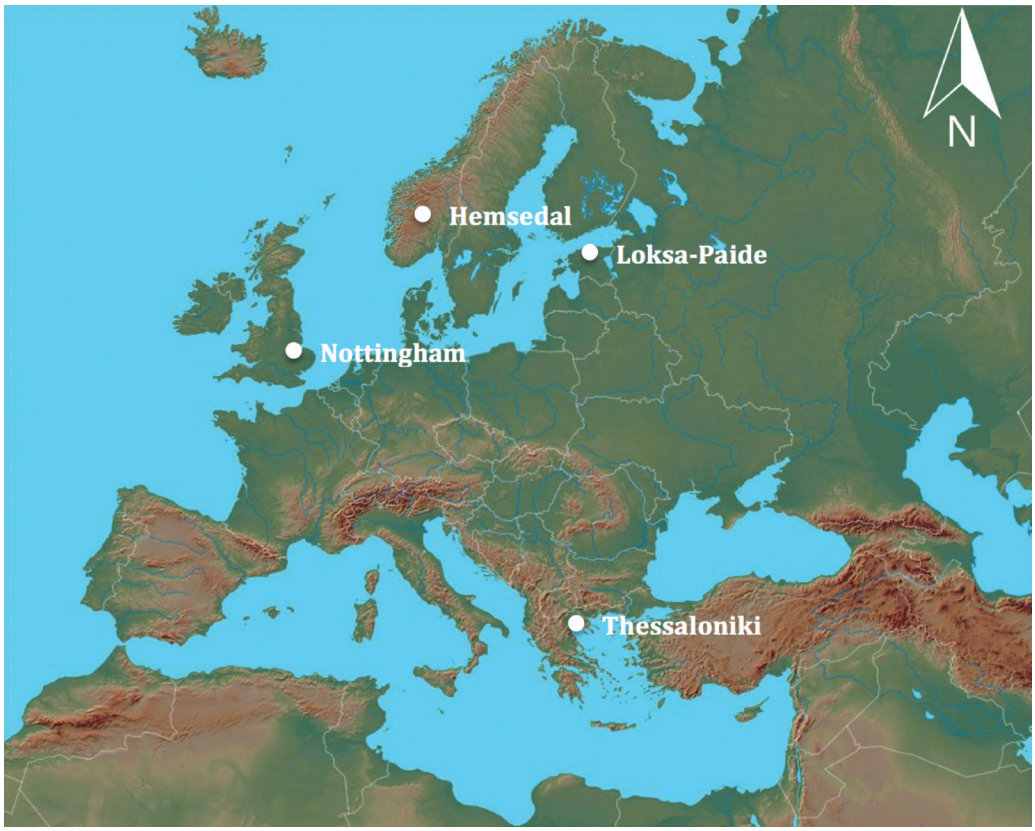

Fig. 1 Study areas across Europe (Geology.com 2016).

1.2 Overview of main SAR characteristics

What occurs when the antenna that transmits is also the one that receives the resulting single-signal power (for cases of point targets) is explained by Eq. 1 (Toomay and Hannen 2004), which denotes the relationship between the different parameters:

$$P_r = \frac{P_t G^2 \lambda^2 \sigma}{(4\pi)^3 R^4}, \quad (1)$$

where:
P_r = power received (watts),
σ = target radar cross section square meters (m^2),
P_t = power transmitted (watts),
G = antenna gain (dimensionless),
R = radar to object range (m),
λ = wave length (m).

In Eq. 1, the first part of the fraction $\left(\frac{P_t G^2}{(4\pi)^3}\right)$ depends on the system and along with the second part $\left(\frac{\lambda^2}{R^4}\right)$, which is related to the signal propagation, it can be determined by calibration procedures. Thus, the remaining coefficient (σ) contains the highest level of uncertainty and is also the most interesting one for the purposes of this study.
In the case of an extended target, such as the area (A) of the resolution cell/pixel of the radar, "σ" is represented by the backscattering coefficient (σ^0), which is the average value of the radar reflective area per area unit $\left(\frac{d\sigma}{dA}\right)$, expressed in m^2/m^2. As a result, Eq. 1 can be modified as follows:

$$P_r = P_t (\sigma^0 A) \left(\frac{G^2 \lambda^2}{(4\pi)^3 R^4}\right), \quad (2)$$

As per the parameter of coherence, consider the simple geometry shown in Fig. 2, including two radar sensors (SAR_1 and SAR_2) with a zero baseline, look angle (θ), along-track distance (x), across-track distance (y), radial distance (r), vertical elevation above the surface (z), center of the radar resolution cell (O) and location (P) of the resolution cell at an arbitrary coordinate (x, y, z). If c is the correlated part of the signal and n the uncorrelated noise due to baseline, thermal, rotation, temporal and other unknown factors, then the measure for the calculation of the complex correlation coefficient γ (i.e. related to coherence) for radar data of the first and second acquisition (s_1 and s_2) is:

$$\gamma = \frac{|\langle s_1 s_2^* \rangle|}{\sqrt{\langle s_1 s_1^* \rangle \langle s_2 s_2^* \rangle}}, \quad (3)$$

where $s_1 = c + n_1$ and $s_2 = c + n_2$ (s^* represents the complex conjugate).

The main components contributing to the total decorrelation are: 1) thermal ($\gamma_{thermal}$ or γ_{SNR}), 2) spatial ($\gamma_{spatial}$ or γ_{proc}) and 3) temporal decorrelation (γ_{temp}).

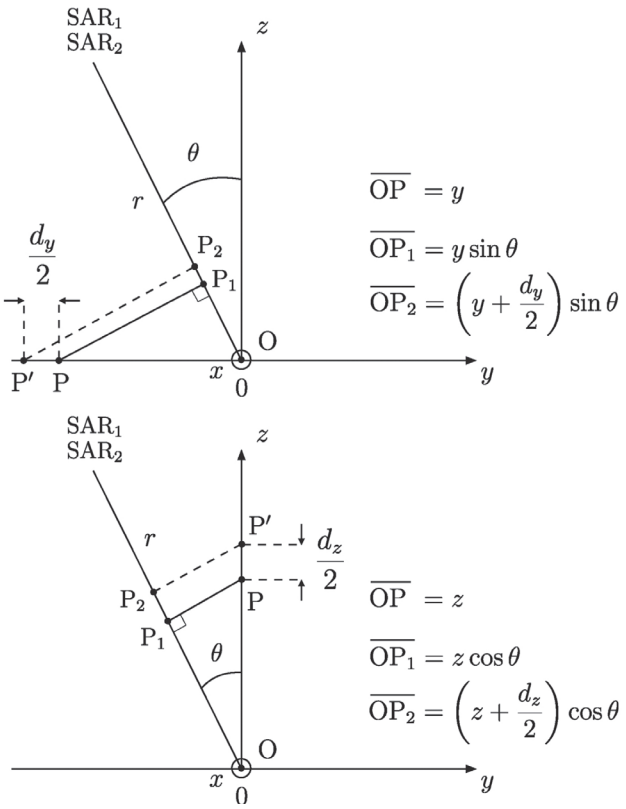

Fig. 2 Resolution cell and imaging geometry of repeat-pass radar interferometer with zero spatial baseline. The *P* point moves into *P'* between the acquisitions, the displacement of P and P'along y and z results in a phase offset that depends on the look angle θ (Lavalle et al. 2012).

The relationship between $\gamma_{thermal}$ and Signal to Noise Ratio (SNR) is (Wei and Sandwell 2010; Zebker and Villasenor 1992):

$$\gamma_{\text{thermal}} = \frac{1}{1+\text{SNR}^{-1}} = \frac{|c|^2}{|c|^2+|n|^2}, \quad (4)$$

Zebker and Villasenor (1992), give the Gaussian distributed temporal de-correlation equation:

$$\gamma_{\text{temp}} = \exp\left[-\frac{1}{2}\left(\frac{4\pi}{\lambda_{\text{eff}}}\right)^2\left(\sigma_y^2\sin^2\theta+\sigma_z^2\cos^2\theta\right)\right], \quad (5)$$

where $\lambda_{eff} = \frac{4\pi}{k}\cos\theta$, which introduces another type of correlation, due to the rotation of the target in relation to the radar look direction:

$$\gamma_{\text{rotation}} = -\frac{2\sin\theta|d\varphi|R_x}{\lambda}, \quad (6)$$

where $d\varphi = \varphi_1 - \varphi_2$ is the distance after the small rotation.

Many parameters appear in the various situations, when researchers attach different notability to these components, such as Santoro et al. (2007), by decomposing the γ_{spatial} to $\gamma_{surface}$ and γ_{volume}, because two images taken from different angles are being used. Furthermore, Siqueira et al. (2014), in order to be able to study flora through interferometry, calculates $\gamma_{obs\ (observation)}$ as,

$$\gamma_{\text{vol(volume)}} = \frac{\gamma_{\text{obs}}}{\gamma_{\text{SNR}}\gamma_{\text{spatial}}\gamma_{\text{temp}}} = f(h_v), \quad (7)$$

where $h_v = f^{-1}(\gamma_{vol})$ and $\gamma_{vol} \leq \sin c\left(\frac{k_z h_v}{2}\right)$, while k_z is the vertical wavenumber and h_v flora (e.g. tree) height. An InSAR system requires a pair of images taken from two different points of space, called S_1 and S_2 respectively. These two images must be co-registered and range filtered for uncommon parts of the spectra of S_1 and S_2, in order to increase the coherence (ρ):

$$\rho = \frac{E\{S_1 S_2^*\}}{\sqrt{E\{|S_1|^2\}E\{|S_2|^2\}}}, \quad (8)$$

where E is the expectation value, |.| represents the absolute value, * refers to the complex conjugation, and the processes S_1, S_2, and $S_1S_2^*$ are assumed stationary and jointly stationary. Assuming that there are no multiple realizations of the images and $S_1S_2^*$ are ergodic, and with m and n referring to the image dimensions, while M and N refers to the averaged pixels in each dimension, then:

$$\hat{\rho}_{\text{MLT}} = \frac{\sum_{m=1}^{M}\sum_{n=1}^{N} S_1(m,n)\,S_2^*(m,n)}{\sqrt{\sum_{m=1}^{M}\sum_{n=1}^{N}|S_1(m,n)|^2\sum_{m=1}^{M}\sum_{n=1}^{N}|S_2(m,n)|^2}} = \frac{|\langle s_1 s_2^*\rangle|}{\sqrt{\langle s_1 s_1^*\rangle\langle s_2 s_2^*\rangle}}, \quad (9)$$

where $|\hat{\rho}_{MLT}|$ corresponds to the maximum likelihood estimator of $|\rho|$. The calculation of the coherence |ρ| is possible for any type of multi-dimensional SAR data, as Interferometric Synthetic Aperture Radar (InSAR) or Polarimetric Synthetic Aperture Radar (PolSAR) (Martinez and Pottier 2005).

2. Methodology

2.1 Urban Areas

Typically, the built environment and the stable man-made structures within urban areas are characterized by high coherence (no or little change), as a result of the preservation of SAR signal phase. On the other hand, low coherence due to phase decorrelation may correspond to agricultural areas, dense high-growing vegetation (forest), layover areas and areas of low backscatter (smooth surfaces or steep back-slopes) (Barbieri and Lichtenegger 2005).

The selected data were acquired over the city of Thessaloniki, Greece, with about 1 million residents

Fig. 3 Study area 1: urban environment in Thessaloniki, northern Greece.

in its Larger Urban Zone (LUZ). More than 790 thousands of them are living in the main urban area, which covers about 112,000 km^2, while the construction network and build-up areas are very dense (Fig. 3). Elevations in the area range from MSL (Mean Sea Level) up to 1201 meters (Hellenic Statistical Authority 2011).

The methodology used for the urban areas refers to co-registered images of ascending and descending passes. More specifically, the SAR signal stability for an urban area is analyzed, by averaging the coherence of the two different passes.

Four ascending and six descending ASAR data during 2005 were used. Firstly, the methodology sequence (Fig. 4) consisted of a separate coregistration of the ascending and descending datasets, after applying precise orbits. Consequently, two different coregistered stacks were created – one for ascending and one for descending pass – and then the average coherence was estimated for each of the two passes. The coherence window size was 10 pixels (azimuth) × 2 pixels (range).

In order to maximize the coherence differences between urban and non-urban areas, a multiplication process took place in two steps. Initially, after studying the relevant histograms and identifying the minimum coherence values for each pass, all the pixels were multiplied with the same integer number, in order to obtain values higher than one. That is, if e.g. the minimum coherence was 0.015 then it was multiplied by 100, in order to obtain a value higher than 1 (0.015 × 100 = 1.5). Subsequently, each resulting image was multiplied by itself as many times as considered adequate to achieve the desired enhanced output. That is, the multiplication power depended on the coherence value differences between urban and non-urban areas, i.e. the smaller the original difference the higher the power of multiplication needed to maximize it. For better visualization purposes, the image contrast was also manipulated accordingly. In the next step the two products were orthorectified.

Ultimately, a secondary product was computed, i.e. the average coherence from both ascending and descending data at a resolution of 20 m × 20 m, which

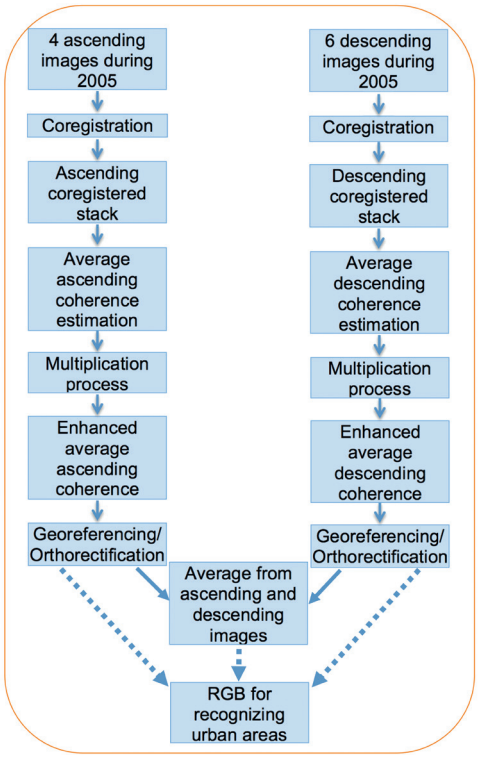

Fig. 4 Methodology followed for the identification of urban areas.

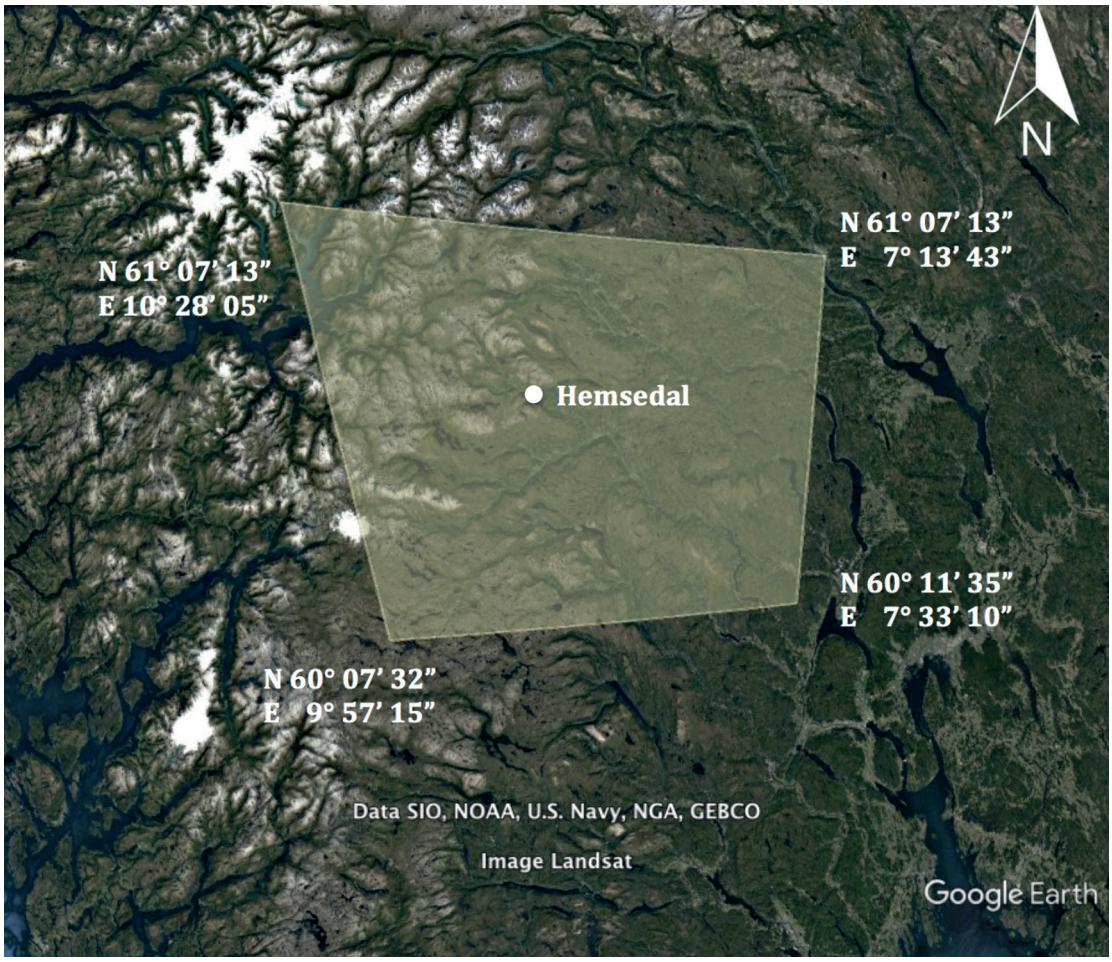

Fig. 5 Study area 2: mountainous terrain near Hemsedal, Norway.

was also used in the creation of an ensemble RGB product for recognizing urban areas.

2.2 Mountainous Terrain

For the analysis of mountainous terrain that is covered by snow or ice, images from Norway and especially images taken near the area of Hemsedal (Fig. 5) have been chosen for backscatter analysis.

In order to increase the reliability of the results, data for three years have been incorporated, i.e. from 2003 to 2005. Taking climatic conditions into account, the acquisition dates of these images were separated in three periods; a) from January to February b) from July to August and c) during May. Both ascending and descending passes were used.

The first period corresponds to winter conditions, during which the mountains in the area are covered by snow and ice. The second period concerns summer conditions, characterized either by high soil moisture content (stemming from the melted snow and ice) or by the presence of bare rocks. In this respect, relatively high backscatter values are expected in the aforementioned two periods (Lu and Meyer 2002). Regarding May, according to the World Weather & Climate Information (2014), it is the driest month in the area, hence significantly lower backscatter values are to be expected.

In order to distinguish the backscatter differences and observe their monthly variances, both descending and ascending passes were used. Separated into semesters and pass type, the images were calibrated, resulting in the calculation of actual backscatter values in db (decibel). Subsequently images were coregistered and orthorectified and statistics were exported for each image category (asceding-descending) (Fig. 6).

The most important element in the analysis is the Snow Water Equivalent (SWE), because of the information on the differences in the backscatter that it

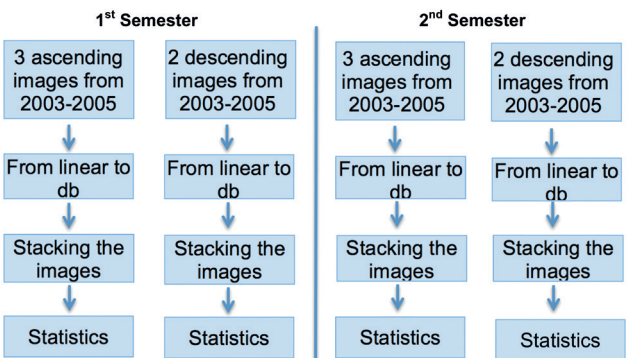

Fig. 6 Methodology followed over mountainous areas.

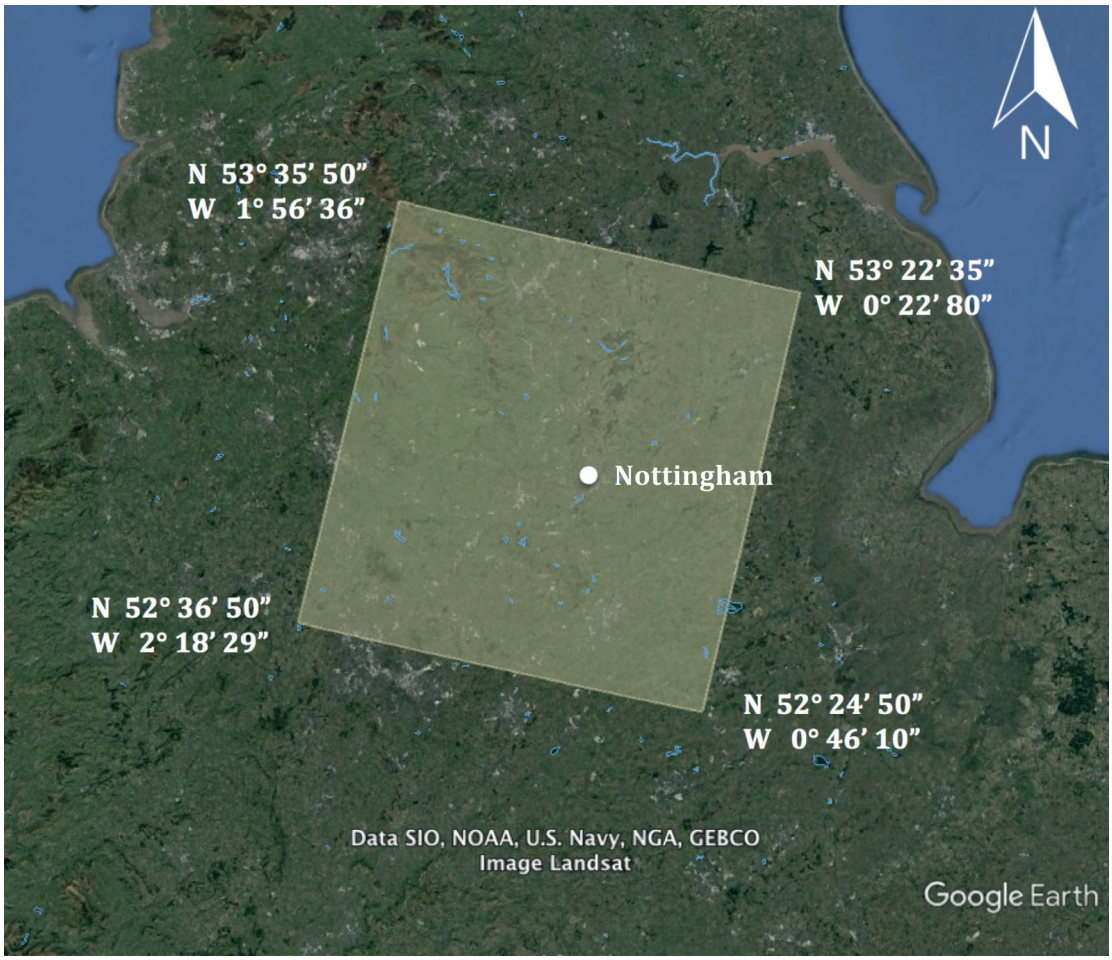

Fig. 7 Study area 3: agricultural and low vegetation in the vicinity of Nottingham, UK.

provides (Storvold et al. 2006). A set of experiments carried out by using ERS-1 data (5.3 GHz, 23° incidence angle) in the Norwegian mountains, has shown that the Snow Covered Area (SCA) could be monitored, as – in special conditions – the snow-free terrain gives high backscatter. Nevertheless, these conditions are very rare and for operational purposes it is better not to use the aforementioned incidence angle of ERS (Solberg 1993). In most cases the snow-covered terrain gives slightly higher backscatter compared to bare ground, but it also depends significantly on the incidence angle and on the snow wetness; "semi-wet" snow results in slightly reduced backscatter (Malnes and Guneriussen 2002).

2.3 Agricultural And Low Vegetation Areas

In order to take sample images of agricultural and low vegetation areas, one such area near Nottingham, UK, has been chosen. One reason for this choice lies in the fact that in the UK agriculture occupies approximately 70% or 9.2 million hectares of its territory (BBC 2007).

Based on the image availability from Envisat ASAR and Land Cover (LC) maps of 2007 (Morton et al. 2011), the area of Central East UK was selected, including most of the Midlands and a little of Eastern areas. The highest point in these areas is Kinder Scout, with 636 meters elevation and an average altitude of almost 150 meters (Fig. 7).

Maps of agricultural production of the years 2000 and 2010 were used (Defra 2006, 2013). Although there are no maps available for the period 2007–2009 (which corresponds to the SAR image dates), it can be assumed that there are no significant changes in agricultural production between 2000 and 2010.

The major part of agricultural production consists of wheat, barley and maize, followed by oilseed rape and potatoes, while sugar beet, potatoes, peas and field beans are also being farmed (Defra 2013, UK Agriculture 2014). The cultivation and harvesting season for the main four products is shown in Table 1.

Tab. 1 The harvesting and cultivation periods for the products studied.

Products	Harvesting period	Cultivation period
Wheat	August	October
Barley	June	October
Maize	April	September
Oilseed rape	Late July	Late August

Source: UK Agriculture, 2014

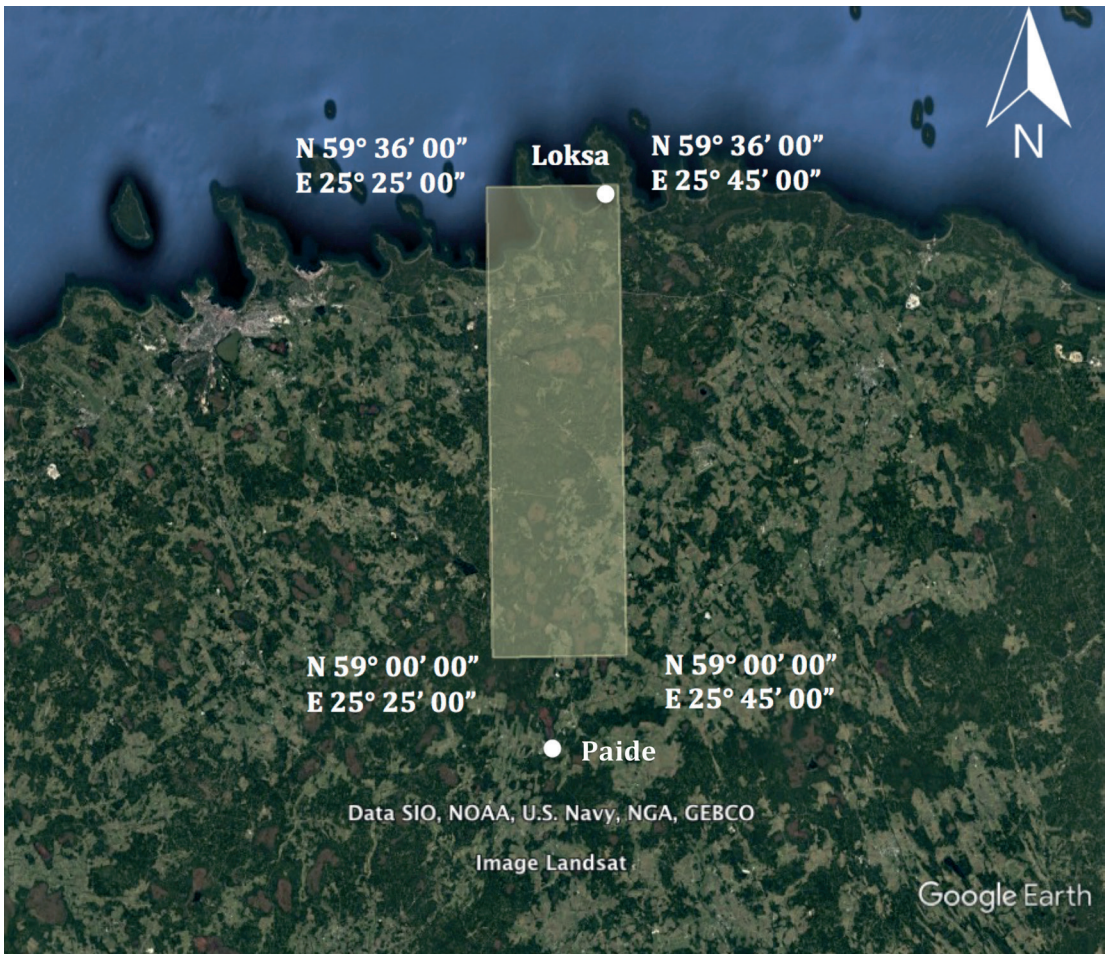

Fig. 8 Study area 4: forested area in Estonia.

Different varieties of wheat and barley exist, such as vernal or winter varieties, with their own production cycles. Cereals constitute the main product of the United Kingdom's crops (Defra 2006), with the most popular of them being the spring wheat which makes up 95% of the total production, opposed to the 5% of the winter wheat's production (Nabim 2014).

For this reason, the selected SAR image acquisition periods were between May and June, representing the backscatter from the products before the harvest. Conversely, the images taken between September and October correspond to the backscatter of the products after the harvest. The analysis focused on the behaviour of backscatter values over several years.

More specifically, from a total of 27 available SLC Envisat/ASAR images, 17 were retrieved during the period between November 2007 and November 2009. From the remaining ten images, five of them refer to the months of May and June for the period from 2004 to 2006, while the remaining five refer to the months of September and October of the same years.

All the images were calibrated and terrain corrected, while backscatter statistics were retrieved for each of the 17 images. The remaining two sets of 5 images were stacked, in order to calculate the average backscatter for each set.

2.4 Forested Areas

The study area is located between the towns of Kehra and Tapa in Estonia (Fig. 8). Although small in extent, Estonia has a large part of its area covered with forest – 2.3 million hectares – which is 51.5% of the mainland territory. The dominant tree species of the Estonian forests are Scots pine (covering 32% of the forested area), followed by birch species (31%), Norway spruce (19%), grey alder (8.5%) and aspen (5%) (Nordic Forest Research 2004).

One of the most important factors that have to be taken into account when studying a forested area with SAR is the wavelength of the available band. Depending on the wavelength used, the penetration of the SAR signal may vary, similarly to other vegetated or agricultural areas (Fig. 9). Thus the information retrieved may be misleading, if not properly interpreted.

For this land cover type nine sets of two images (C band and VV polarization) from the tandem mission of ERS-1 and ERS-2 were chosen and processed for interferometric analysis (coherence estimation and evaluation). From the total of nine available ERS tandem pairs originally processed, only four were eventually selected for further analysis.

From this set of four pairs, two were acquired around the summer period, while the other two were

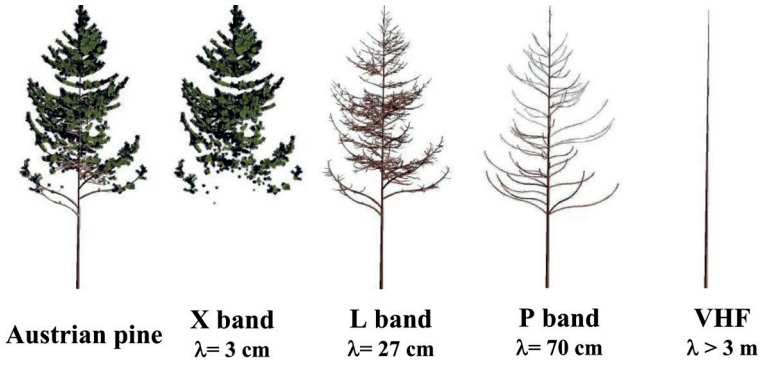

Fig. 9 Dependence of SAR backscatter of biomass (leaves, branches, trunks) from the radar wavelength (Le Toan 2007; Le Toan et al. 2001).

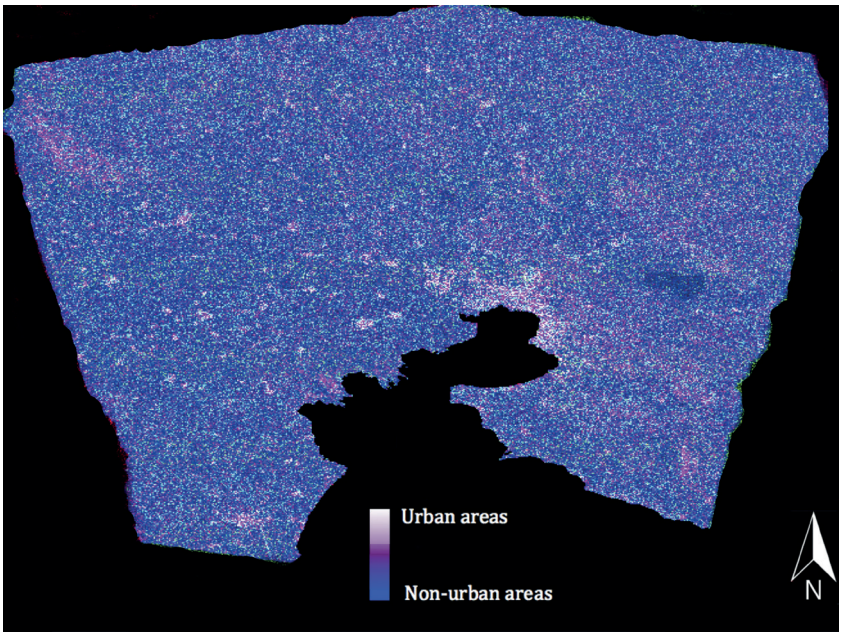

Fig. 10 RGB image of Thessaloniki area, produced by the average coherence of 4 ascending and 6 descending SAR images (Red: average of descending pass; Green: average of ascending pass; Blue: average of both passes).

acquired during winter. The fact that the images were spread during two semesters provided the opportunity to study the area during two extreme conditions. These conditions also represent the extremes in the trees' annual life cycle (especially for deciduous trees) – being devoid of foliage (winter) and full of foliage (summer).

3. Results and Discussion

3.1 Urban Areas

Concerning the urban versus non-urban areas, an attempt to classify them based on coherence, showed considerably higher values for the former and lower values for the latter, as represented in the final orthorectified RGB product (Fig. 10). The higher backscatter values of the urban areas are something to be expected, as there are many corner reflectors for the SAR signal within the built environment.

Furthermore, by having a pair of images or a series of images taken over a considerable period of time, one can further estimate the construction activity of an area.

3.2 Mountainous Areas

In the analysis of this study area it was highlighted how the backscatter variation is connected to each semester and the related weather conditions. In the first semester the mean backscatter value is the highest of the year, possibly due to the high volume of snow- or ice-covered terrain. On the other hand, in the second semester, most of the mountain area is snow-free, which results in lower backscatter values in the area, compared to the winter period.

Finally, in May images, the backscatter has the lowest values of the year. By studying the specific month, a "snowline" can be identified between the highest parts – where there is continuous snow cover – and the lowest parts of the basin – where there

is snow-free ground as well (Andersen 1982). Bearing this in mind, experiments in three subsets of the average May image were carried out, in order to study the backscatter values at three respective altitude zones. The results provide some indication on how the backscatter decreases progressively, when moving from the highest part of the mountains to lower elevations, but further investigation and more data is needed, in order to come to meaningful conclusions.

3.3 Agricultural and Low Vegetation Areas

Regarding the agricultural and low vegetation areas, taking into account annual rainfall data, the interpretation of backscatter variation is based on soil moisture and roughness variations. When these two variables have low values (dry and smooth surface), the backscatter is also low. When either of the two parameters is characterized by high values (wet and/or rough surface), the resulting backscatter is high.

Thus the reason why the backscatter in winter is high can be attributed to the increased soil moisture. During winter months, the agricultural production is not fully-grown and most of the SAR signal returns directly from the ground, which is also wet, resulting in high backscatter values. It ought to be noted that this behavior is similar to that of trees; before the signal returns to the receiver, it can follow different pathways, which may thus result in different backscatter values.

In more detail, as it can be observed in Fig. 11, from March to September, the average image backscatter has the lowest values. From November to February, the values start to rise.

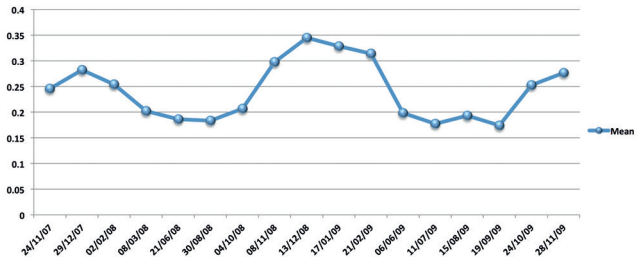

Fig. 11 Periodicity of the mean backscatter values for the agricultural and low vegetation areas.

Additionally, from the two sets of 5 images the typical backscatter values before and after the harvest for the agricultural areas were calculated; the most distinct differences can be observed in terms of mean values for the May/June (0.1428+/−0.0528) and September/October (0.2447+/−0.0766). These values and periodicity can be attributed to the backscatter variations of crops rather than urban areas, as shown in Fig. 12.

Taking into consideration the different stages of growth for each crop type (Fig. 13), as well as the average monthly precipitation in the study area (Fig. 14), further investigation could be performed. This ought

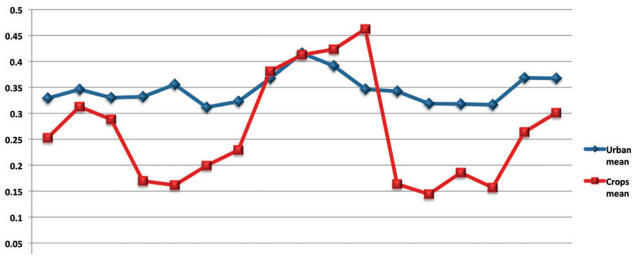

Fig. 12 Comparison of the mean backscatter values for crops and urban areas.

to focus on the backscatter variations, owing to the changes in the two main factors affecting the SAR signal, i.e. surface roughness and dielectric constant (directly related to the water content). Nevertheless, this would require extensive in-situ data and an analysis per crop type, as their cultivation periods differ significantly.

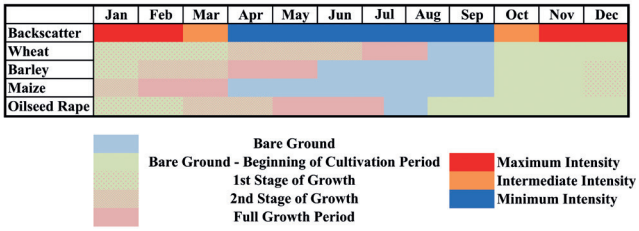

Fig. 13 Monthly backscatter with respect to the different stages of growth, for each crop type.

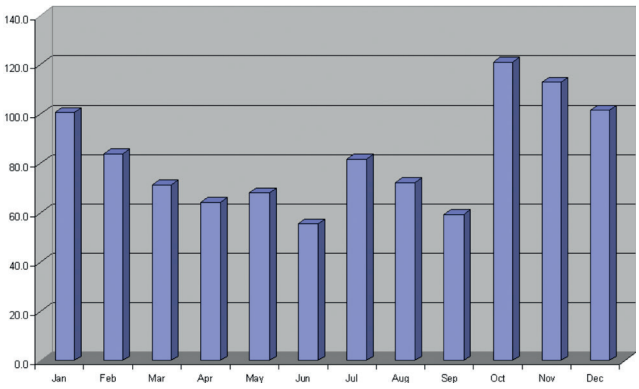

Fig. 14 Average monthly precipitation for study area 3 (agricultural and low vegetated area).

3.4 Forested Areas

Finally, for the forested areas, the coherence results for the two winter datasets, show a concentration of the pixel values between 0.4 and 0.7, with a maximum accumulation at 0.65 and a mean value of 0.51. On the other hand, for the summer image sets, the pixel values are concentrated between 0.2 and 0.35 with a maximum accumulation at 0.25 and a mean value of 0.35. Especially for August and February, greater data dispersion was identified, with many pixels having values up to 0.7 and down to 0.4 respectively. Furthermore, the pixels values from the two sets of

coherence were averaged, in order to get the mean values for each pixel for each semester.

Subsequently, using the CORINE land cover database (scale of 1 : 100,000) and the processed coherence images, all the relevant classes and their coherence could be identified in a GIS (ArcGIS™) for each semester (Table 2).

As regards to the coherence for the forested areas (coniferous, mixed and broad-leaved), the results show that during summer the values are characteristically lower compared to the other classes. Furthermore, even though coherence increases during winter, it has still lower values for the aforementioned forested areas than in the other classes, but with a wider range. Between the different species, low coherence results throughout the year are encountered (from lowest to highest) over coniferous forests, followed by mixed, broad-leaved forest and finally transitional woodland shrub. For the different species, lower coherence was also associated with higher dispersion.

Tab. 2 Summer and winter coherence for the different classes.

Class	Summer Coherence	Winter Coherence
Inland marshes	0.48–0.64	0.57–0.73
Transitional woodland shrub	0.32–0.67	0.53–0.83
Pastures	0.22–0.51	0.44–0.77
Land occupied by agriculture	0.20–0.66	0.37–0.77
Mixed forest	0.12–0.45	0.22–0.70
Coniferous forest	0.09–0.66	0.14–0.78
Water bodies	0.16–0.49	0.53–0.74
Industrial or commercial units	0.25–0.46	0.32–0.58
Mineral extraction sites	0.45–0.65	0.55–0.79
Discontinuous urban fabric	0.21–0.55	0.35–0.71
Non-irrigated arable land	0.37–0.68	0.55–0.81
Complex cultivation patterns	0.36–0.70	0.45–0.77
Broad-leaved forest	0.20–0.57	0.34–0.74
Natural grassland	0.30–0.50	0.40–0.78
Peat bogs	0.34–0.74	0.44–0.82
Moors and heathland	0.22–0.53	0.49–0.73
Road and rail networks	0.44–0.54	0.58–0.74

4. Conclusions

In this paper, different approaches for land cover monitoring through classification with the use of SAR data were tested over Europe. In particular, ERS and Envisat/ASAR datasets were employed in order to identify urban, mountainous, agricultural/low vegetation areas and forests, by exploiting SAR backscatter and coherence. The period of SAR observations included data from all four seasons, thus covering a variety of meteorological conditions, as well as agricultural/vegetation stages.

For the urban and non-urban areas an attempt to classify them based on coherence, showed great value differences between the two aforementioned categories. For the selected location, images throughout the year were used and no deterioration of the results due to moisture or rain was observed. On these grounds, it can be assumed that this methodology is robust enough to be used for studies related to urban sprawl monitoring.

On the other hand, in the case of the mountainous areas at high latitudes under study, it has proven difficult to separate the mountainous snow-free terrain from the snow-covered, without weather information. The results for winter/summer show little difference between the mean, maximum and minimum backscatter. The reason is that in the first semester (winter) the mountains are full of snow, while in the second semester (summer) the snow and ice are melted and stagnated in the area. As a result, a relatively high backscatter is observed during both semesters. Nevertheless, during May, which is the driest month of the year in the study area, backscatter values are significantly lower. Consequently, during this period, it may be relatively easy to use backscatter values for snow line mapping, if considerably more satellite images are employed.

Regarding the agricultural and low vegetation areas, the interpretation of results ought to be performed in conjunction with the annual rainfall in the UK and by considering soil moisture and roughness. Especially with respect to the relative weight (importance) of these two last parameters, which are critical for SAR backscatter, this case study from the area in the UK has provided with some interesting insights.

More specifically, in this case study, winter backscatter values of agricultural areas were high, while the respective summer values were relatively low.

This information should be combined with the fact that during winter, surface roughness is low (theoretically low backscatter), as the agricultural areas have been harvested and seeded for the next growth period, while soil moisture is high (theoretically high backscatter).

On the contrary, during summer, the surface is rather rough, as the agricultural production is fully grown (theoretically high backscatter), while soil moisture is relatively low (theoretically low backscatter).

Therefore, it seems that for agricultural and low vegetation areas, soil moisture is a more important factor than roughness and it more or less determines the strength of SAR backscatter.

In any case, working with this type of terrain requires more in-situ information, also taking into account daily meteorological data and the agricultural cycle of different crops.

Finally, for the forested areas, a methodology based on Corine Land Cover (CLC) maps has been adopted; in order to classify all the areas based on backscatter and coherence values and to discover the differences

between the various forest types. Common ground for all of these kinds of forest is the low coherence and the high variability, all over the year, in relation to all the other types of land cover. Therefore, it is relatively easy to discriminate forest from non-forested areas. On the other hand, the coherence values of the different types of forest are very similar (between 0.09–0.67 for the summer and 0.14–0.83 for the winter). Thus, in order to discriminate between different types of forest, in-situ information and/or different kind of SAR data (more polarizations) is needed.

In conclusion, the heritage and experience gained from ERS and Envisat/ASAR SAR imaging for land cover classification approaches shall be invaluable for the exploitation of current and future SAR data. In the European context in particular, the Sentinel-1 satellites (since 2014) within the realization of the Copernicus Programme, guarantee not only the continuity of European C-band SAR satellite missions, but also bring along significant improvements. These are mainly in terms of spatial and temporal resolution, as well as systematic acquisitions in at least two polarizing modes, resulting in an overall improved capability of monitoring land surface and discriminating between different land cover types.

Acknowledgements

This study could not have been completed without the various SAR data from ENVISAT and ERS-1/2, for which the European Space Agency (ESA) provided access through EOLiSA, in the framework of a category-1 project (ID: 28350). The first author would also like to thank Dr. Stephen Hobbs and Dr. Konstantinos Salonitis, for giving him the opportunity to realize this study as part of his thesis at the Department of Aeronautics and Space Engineering of Cranfield University, but also for taking part in the project GEoSTARe.

References

Ackermann, R. E. (2011): Sequential land cover classification (unpublished MSc thesis), University of Pretoria, South Africa.

Andersen, T. (1982): Operational snow mapping by satellites. Hydrological Aspects of Alpine and High Mountain Areas. Proceedings of the Exeter Symposium, July 1982, IAHS Publication 138, 149–154.

Barbieri, M., Lichtenegger, J. (2005): Introduction to SAR for Geology. In K. Fletcher (ed), Spaceborne radar applications in Geology, ESA TM-17: 1–54, Noordwijk, European Space Agency.

BBC (2007): Snapshot of farming in the UK. http://news.bbc.co.uk/2/hi/uk_news/magazine/6919829.stm

DEFRA (2006): Arable crops grown in the UK. http://archive.defra.gov.uk/foodfarm/growing/crops/

DEFRA (2013): Farming statistics provisional crop areas, yields and livestock populations at June 2013. United Kingdom, National Statistics Publications. https://www.gov.uk/government/uploads/system/uploads/attachment_data/file/364157/structure-jun2013prov-UK-16oct14.pdf

Geology.com (2016): Physical map of Europe. http://geology.com/world/europe-physical-map.shtml

Haack, N. B., Herold, D. N., Bechdol, A. M. (2000): Radar and optical data integration for land-use/land-cover mapping. Photogrammetric Engineering and Remote Sensing 66(6), 709–716. http://asprs.org/a/publications/pers/2000journal/june/2000_jun_709-716.pdf

Hale, S. R., Rock, B. N., (2003): Impacts of topographic normalization on land-cover classification accuracy. Photogrammetric Engineering and Remote Sensing 69(7), 785–791, https://doi.org/10.14358/PERS.69.7.785.

Hanssen, R. F. (2001): Radar Interferometry: Data Interpretation and Error Analysis, Springer, Berlin, https://doi.org/10.1007/0-306-47633-9.

Hellenic Statistical Authority (2011): Statistical Yearbook of Greece, 2009 and 2010. Piraeus, Greece.

Kaoru, T., Toshiharu, K. (1996): GIS-aided land cover classification assessment based on remote sensing images with different spatial resolutions. Application of Geographic Information Systems in Hydrology and Water Resources Management. Proceedings of the Vienna Conference HydroGIS '96, IAHS Publication 235, 659–665.

Lavalle, M. (2013): Tackling temporal decorrelation in repeat-pass polarimetric interferometry. 2nd Advanced Course on Radar Polarimetry, 21–25 January 2013, ESA-ESRIN. Frascati (Rome), Italy.

Lavalle, M., Simard, M., Hensley, S. (2012): A Temporal Decorrelation Model for Polarimetric Radar Interferometers. IEEE Transaction on Geoscience and Remote Sensing, 50(72012), 2880–2888, https://doi.org/10.1109/TGRS.2011.2174367.

Le Toan, T. (2007): SAR data for forestry and agriculture. Advances Training Course on Land Remote Sensing, 5 September 2007, Lecture D3L3. http://earth.esa.int/landtraining07/D3L3-LeToan.pdf

Le Toan, T., Picard, G., Martinez, J. M., Melon, P., Davidson, M. (2001): On the relationships between radar measurements and forest structure and biomass. Proceedings of the Third International Symposium on Retrieval of Bio- and Geophysical Parameters from SAR Data for Land Applications, 11–14 September 2001, Sheffield, UK. ESA Publications Division (ESA SP-475), Noordwijk, Netherlands, 3–12.

Long, G. D. (2008): Microwave Sensors – Active and Passive. Provo, UT.

Lu, D., Weng, Q. (2007): A survey of image classification methods and techniques for improving classification performance. International Journal of Remote Sensing 28(5), 823–870, https://doi.org/10.1080/01431160600746456.

Lu, Z., MEYER, D. J. (2001): Study of high SAR backscattering caused by an increase of soil moisture over a sparsely vegetated area: implications for characteristics of backscattering. International Journal of Remote Sensing 23(6), 1063–1074, https://doi.org/10.1080/01431160110040035.

Lusch, P. D. (1999): Introduction to Microwave Remote Sensing. Center for Remote Sensing and Geographic Information Science. Michigan State Univesity, BSRSI, November 1999, Michigan, 1-84. http://web.pdx.edu/~emch/ip2/RADAR.pdf

Malnes, E., Guneriussen, T. (2002): Mapping of snow covered area with Radarsat in Norway. Procceedings IGARSS'02, 28 June 2002, Vol. 1, 683–685, Toronto, Canada, https://doi.org/10.1109/IGARSS.2002.1025145.

Martinez, C. L., Pottier, E. (2005): Topography Independent InSAR Coherence Estimation in a Multiresolution Scheme. Proceedings of IEEE International Geoscience and Remote Sensing Symposium, IGARSS '05,25-29 July 2005, Vol. 4, 2689–2692, Seoul, Korea, https://doi.org/10.1109/IGARSS.2005.1525620.

Morton, D., Rowland, C., Wood, C., Meek, L., Marston, C., Smith, G., Wadsworth, R., Simpson, C. I. (2011): Final Report for LCM 2007 – the new UK Land Cover Map. CS Technical Report No 11/07, Countryside Survey, July 2011. http://www.countrysidesurvey.org.uk

NABIM (2014): Wheat Production. http://www.nabim.org.uk/wheat/wheat-production

Nordic Forest Research (2004): Forest Research in the North: Estonia. Scandinavian Journal of Forest Research (News & Views). http://www.nordicforestresearch.org/wp-content/uploads/2011/03/NV_2004_1.pdf

Rhode Hill Gardens (2018). Rainfall at Rhode Hill Gardens. http://homepages.nildram.co.uk/~rhg/rain.html#ad

Santoro, M., Askne, J. H., Wegmuller, U., Werner, C. L. (2007): Observations, Modeling, and Applications of Ers-Envisat Coherence Over Land and Surfaces. Geoscience and Remote Sensing, IEEE Transactions 45(8), 2600–2611, https://doi.org/10.1109/TGRS.2007.897420.

Siqueira, P., Hensley, S., Chapman, B., Bergen, K.: Temporal decorrelation studies relevant for a vegetation InSAR mission, NASA, (unpublished poster). http://cce.nasa.gov/mtg06_ab_presentations/163_138_ab_pres.pdf

Sokal, R. (1974): Classification: purposes, principles, progress, prospects. Journal Science 185(4157), 1115–1123, https://doi.org/10.1126/science.185.4157.1115.

Solberg, R. (1993): Mapping Snow Cover by ERS-I SAR. Proceedings of IGARSS '93 Symposium, Vol. 3, 1273–1275, Tokyo, Japan. https://doi.org/10.1109/IGARSS.1993.322100.

Song, C., Woodcock, C. E., Seto, K. C., Lenney, M. P., Macomber, S. A. (2001): Classification and change detection using Landsat TM data: when and how to correct atmospheric effect. Remote Sensing of Environment 75(2), 230–244, https://doi.org/10.1016/S0034-4257(00)00169-3.

Storvold, R., Malnes, E., Larsen, Y., Høgda, A. K., Hamran, E. S., Muller, K., Langley, A. K. (2006): SAR Remote Sensing of snow parameters in Norwegian areas – current status and future perspective. Journal of Electromagnetic Waves and Applications 20(13), 1751–1759. https://doi.org/10.1163/156939306779292192.

Toomay, J. C., Hannen, J. P. (2004): Radar principles for the Non-specialist. 3rd Edition, Scitech Publishing, New York, https://doi.org/10.1049/SBRA032E.

UK Agriculture (2014): Crops in the UK. http://www.ukagriculture.com/crops/crops.cfm

Wei, M., Sandwell, T. D. (2010): Decorrelation of L-Band and C-Band Interferometry Over Vegetated Areas in California. IEEE Transaction on Geoscience and Remote Sensing 48(7), 2942–2952, https://doi.org/10.1109/TGRS.2010.2043442.

World Weather & Climate Information (2014): Average weather in Bergen, Norway. http://www.weather-and-climate.com/average-monthly-Rainfall-Temperature-Sunshine,bergen,Norway

Zebker, A. H., Villasenor J. (1992): Decorrelation in Interferometric Radar Echoes. IEEE Transaction on Geoscience and Remote Sensing 30(5), 950–959, https://doi.org/10.1109/36.175330.